Elucidation of Adsorption Mechanisms And Mass Transfer Controlling Resistances During Single And Binary Adsorption of Caffeic And Chlorogenic Acids

Eyden S. Hernández-Padilla
Universidad Autónoma de San Luis Potosí: Universidad Autonoma de San Luis Potosi
Ana I. Zárate-Guzmán
Universidad Autónoma de San Luis Potosí: Universidad Autonoma de San Luis Potosi
Omar González-Ortega
Universidad Autónoma de San Luis Potosí: Universidad Autonoma de San Luis Potosi
Erika Padilla-Ortega
Universidad Autónoma de San Luis Potosí: Universidad Autonoma de San Luis Potosi
Azael Gómez-Durán
Universidad Autonoma de San Luis Potosi Facultad de Ciencias Quimicas
Pablo Delgado-Sánchez
Universidad Autonoma de San Luis Potosi Facultad de Agronomia y Veterinaria
Angélica Aguilar-Aguilar
Universidad Autonoma de San Luis Potosi Facultad de Ciencias Quimicas
Farid B. Cortés
Universidad Nacional de Colombia Sede Medellín: Universidad Nacional de Colombia Sede Medellin
Raul Ocampo-Perez (raul.ocampo@uaslp.mx)
Universidad Autonoma de San Luis Potosi

Research Article

Keywords: Caffeic acid, chlorogenic acid, binary adsorption, granular activated carbon.

Posted Date: August 23rd, 2021

DOI: https://doi.org/10.21203/rs.3.rs-802929/v1

ELUCIDATION OF ADSORPTION MECHANISMS AND MASS TRANSFER CONTROLLING RESISTANCES DURING SINGLE AND BINARY ADSORPTION OF CAFFEIC AND CHLOROGENIC ACIDS

Eyden S. Hernández-Padilla[a], Ana I. Zárate-Guzmán[a], Omar González-Ortega[a], Erika Padilla-Ortega[a], Azael Gómez-Durán[a], Pablo Delgado-Sánchez[b], Angélica Aguilar-Aguilar[a], Farid B. Cortés[c], Raúl Ocampo-Pérez [a*]

[a]Centro de Investigación y Estudios de Posgrado, Facultad de Ciencias Químicas, Universidad Autónoma de San Luis Potosí, San Luis Potosí 78260, México.

[b]Laboratorio de Biotecnología, Facultad de Agronomía y Veterinaria, Universidad Autónoma de San Luis Potosí, Soledad de Graciano Sánchez, San Luis Potosí, Mexico.

[C]Grupo de Investigación en Fenómenos de Superficie – Michael Polanyi, Facultad de Minas, Universidad Nacional de Colombia-Sede Medellín, Colombia.

*To whom correspondence should be addressed: Tel: 52-4448132157. e-mail: raul.ocampo@uaslp.mx.

HIGHLIGHTS

- Adsorption and mass transfer mechanisms of phenolic acids on GAC was elucidated.
- Adsorption of both acid compounds was governed by π-π and electrostatic interactions
- Binary adsorption of caffeic acid and chlorogenic acid is antagonistic in nature
- Pore volume and surface diffusion mechanisms play an important role during adsorption

54

55 **NOMENCLATURE**

C_A = Concentration of CA or CGA in aqueous solution, mmol/L.

C_{A0} = Initial concentration of CA or CGA in aqueous solution mmol/L.

C_{Ae} = Concentration of CA or CGA at equilibrium, mmolg/L.

C_{AP} = Concentration of CA or CGA within the particle, mmolg/L.

$C_{AP}|_{B_{p-s}}$ = Concentration of CA or CGA at the external surface of the particle (r = R), mmol/L.

D_{ep} = Pore volume diffusion coefficient, cm^2/s.

D_s = Surface diffusion coefficient, cm^2/s.

D_{AB} = Molecular diffusion coefficient at infinite dilution, cm^2/s

k_L = External mass transfer coefficient in liquid phase, cm/s.

K_E = Affinity of the adsorbent for compound i

m = Mass of adsorbent, g.

N_{AP} = Mass transport due to pore volume diffusion, mg/cm^2-min.

N_{AS} = Mass transport due to surface diffusion, mg $/cm^2$-min.

q Mass of CA or CGA adsorbed predicted with the adsorption isotherm, mmol/g.

q_{exp} Experimental mass of CA or CGA adsorbed at equilibrium, mmolg/g.

q_e Mass of CA or CGA adsorbed at equilibrium predicted with the adsorption isotherm, mmol/g.

q_{max} Maximum adsorption capacity for the compounds in the binary solution, mmol/g.

R = Average radius of the particle, 0.0542 cm.

S = External surface area per mass of adsorbent, cm^2/g, $S = 3/R\rho_p$.

V = Volume of the solution, mL.

Greek symbols

ε_p = Void fraction of particles

ρ_p = Density of adsorbent particles, g/cm.

τ = Tortuosity factor

56

57

ABSTRACT

In this work, the potential of activated carbon to remove caffeic and chlorogenic acids was investigated. The study focused on evaluating the single and binary adsorption equilibrium, as well as investigating the mass transfer resistances present during the process by applying kinetic and diffusional models for a future scale-up of the process. For both compounds, the single adsorption equilibrium was studied at pH values of 3, 5, and 7. The experimental adsorption isotherms were interpreted using the Langmuir and Freundlich models, obtaining maximum adsorption capacities of 1.33 and 1.62 mmol/g for caffeic and chlorogenic acid, respectively. It was found that the adsorption mechanisms for both compounds was derived from π-π and electrostatic interactions. Also, the binary adsorption equilibrium was performed and the experimental data were interpreted using the extended multicomponent Langmuir model. The results evidenced that the binary adsorption of caffeic acid and chlorogenic acid is antagonistic in nature. The application of the first and second order kinetic models showed that the latter interpreted better the experimental data, obtaining R2 values close to one. Finally, the experimental adsorption rate data were interpreted by a diffusional model, finding the presence of different mass transfer resistances during the adsorption process. For both compounds, intraparticle diffusion mechanisms were meaningful.

Keywords: Caffeic acid, chlorogenic acid, binary adsorption, granular activated carbon**.**

1. INTRODUCTION

Caffeic and chlorogenic acids are phenolic compounds with beneficial properties for the human health; they have potent antioxidant, antiviral, anti-inflammatory, and antirheumatic activities (Singleton and Cilliers 1991). Moreover, both compounds can be used to synthesize drugs to combat neurodegenerative, cardiovascular, or carcinogenic diseases (Chang et al. 2010). These acids are widely distributed in vegetables, fruits, and herbs (e.g. artichokes, peanuts, and cinnamon) (Farah and Donangelo 2006). They are also present in coffee grains of the residual waters derived from the production of coffee (J.E. Braham and R. Bressani 1970).

Mexico possesses the 11th place as coffee producer and the 12th place as exporter with a cultivation area of 1,584,451 acres worldwide (J.E. Braham and R. Bressani 1970). Evidently, this production rate has as consequence an increase in the generation of wastewater derived from the production of coffee. This wastewater has a high content of organic matter with elevated acidity due to the presence of caffeic, chlorogenic, quinic, and acetic acids (J.E. Braham and R. Bressani 1970). Therefore, it is always relevant to evaluate the existent technologies for the remotion of these valuable compounds. In this context, adsorption is a cheap and simple to operate method with a variety of adsorbents that include starch (Simanaviciute et al. 2017), silica (Moritz and Geszke-Moritz 2016), ionic liquids (Du et al. 2011), macroporous resins (Jiang et al. 2020), and chitosan (Liudvinaviciute et al. 2020).

Few studies exist in the literature dealing with the adsorption of caffeic and chlorogenic acids. Furthermore, these studies are focused on the individual adsorption of one of these compounds, ignoring not only the behavior of binary systems but the diffusional effects during the adsorption process. Simanaviciute et al. (2017) evaluated the adsorption,

105 at equilibrium, of caffeic and chlorogenic acids at different temperatures on crosslinked
106 cationic starch. Their results established that the maximum adsorption capacity was 1.5-fold
107 higher for chlorogenic acid than for caffeic acid; moreover, these authors determined that
108 electrostatic interactions played a predominant role during the adsorption of both acids. The
109 adsorption of caffeic acid over the silica SBA-15 and MCF functionalized with APTES (3-
110 aminopropyltriethoxysilane) and AEAPTMS ([3-(2-aminoethylamino) propyl]
111 triimethoxysilane) was investigated by Moritz and Geszke-Moritz (2016) using 2-propanol
112 as solvent. The results established that the adsorption capacity was higher for the AEAPTMS-
113 functionalized SBA-15 and MCF (192.3 and 161.3 mg/g, respectively) when compared to
114 the APTES-functionalized counterparts (125.0 and 113.6 mg/g, respectively). Jiang et al.
115 (2020) studied the equilibrium, kinetics, and desorption of chlorogenic acid in 10 different
116 types of macroporous resins (AB-8, D4020, HPD-722, HPD-300, HPD-100, NKA, NKA-II,
117 NKA-9, S-8, and X-5). The results indicated that polar resins had higher adsorption capacity
118 when compared to nonpolar resins, the resin NKA-II showed the highest adsorption capacity
119 (35.6 mg/g). Finally, these authors showed that the pseudo-second order model properly
120 interpreted the experimental data of adsorption kinetics.

121 Unlike the adsorbents employed in the literature, activated carbon presents high
122 specific area and a variety of functional groups that could enhance the adsorption of caffeic
123 and chlorogenic acids. The caffeic and chlorogenic acids are natural hydroxycinnamic acids
124 that are common in beverages derived from plants such as coffee (Wang and Ho 2009). As
125 consequence, both compounds will exist in water and compete for the adsorption sites in the
126 adsorbent. In a competitive adsorption situation, the adsorption of one component could be
127 diminished, favored, or unaffected by the presence of other components (Srivastava et al.
128 2006); these types of competitive situations are named antagonistic, cooperative or synergic,

and noninteractive, respectively (Carrales-Alvarado et al. 2018). To the best of our knowledge, neither the competitive adsorption of caffeic and chlorogenic acids nor the use of models of multicomponent adsorption have been studied. For this reason, the objective of the present work is to investigate, for the first time, the potential of activated carbon for the removal of caffeic and chlorogenic acids evaluating the individual and binary adsorption. Additionally, the adsorption rate of both compounds was studied in-depth, along with the mass transfer mechanisms during the adsorption process using kinetic and diffusional models for a future scale-up of the process.

2. MATERIALS AND METHODS

2.1. Adsorbates

In this work, caffeic (CA) and chlorogenic (CGA) acids were acquired from Merck, bot with a purity ≥95%. Their physicochemical properties are presented in Table 1. From their values of pKa, the speciation diagrams shown in Figure 1 were constructed. For the case of CGA (Figure 1a), it exists as neutral molecule at pH values < 2, while at a pH value of 3.6; half of the molecules are dissociated (negatively charged) due to deprotonation of the carboxylic group (-COOH). As the pH raises beyond, the CGA molecule is more negative due to deprotonation of the OH group from the catechol moiety ($-C_6H_4(OH)_2$). A similar behavior occurs for CA (Figure 1b).

2.2. Quantification of CA and CGA

The quantification of the individual concentration of CA and CGA in aqueous solution was carried out by UV-Vis spectroscopy using a double-beam spectrophotometer (Shimadzu UV

2600). The absorbance of a CGA solution was measured at 325 nm for the 3-7 pH range, while 322 (pH value of 3) and 287 nm (5-7 of pH range) were used for CA. The quantification of CA and CGA in binary solutions was carried out using and HPLC equipped with a DAD (Agilent model 2998). A 10-min linear gradient was run after sample (or standard) injection (10 µL) using solvents A (0.1% trifluoroacetic acid in water) and B (0.1% trifluoroacetic acid in acetonitrile). Detection was performed at 250 nm using a flowrate of 0.6 mL min^{-1}.

2.3. Adsorbent

A commercial F400 granular activated carbon (GAC) was used as adsorbent; it was a gift from the Calgon Carbon Corp. Before using it, the GAC was sieved through a 30-50 mesh to obtain particles with an average radius of 0.542 mm, which were washed three times with deionized water to eliminate dust and impurities. The GAC washed was afterwards dried at 110°C for 24 h using a conventional model, the material was finally stored in a sealed container. The textural properties of the adsorbent (specific surface area, pore volume, and average pore diameter) were determined by N_2 physisorption at 77 K using a Micromeritics ASAP 2020 equipment. The superficial area (S_{BET}) and micropores volume (V_{mic}) were calculated using the models proposed by Brunauer, Emmett, and Teller (BET) and Dubinin-Radushkevich, respectively. The diameter of the micropores (L_0) was estimated using the equation proposed by Stoeckli (1995) (Stoeckli et al. 1995), while the superficial chemistry was studied by the acid-base titration method proposed by Boehm (1994) (Boehm 1994). Finally, the surface charge of the GAC was determined using the acid-base titration method established by Kuzin and Loskutov (1996) (Kuzin, I. A. y Loskutov 1996).

2.4. Adsorption rate and equilibrium data

The concentration decay curves for CA and CGA on GAC were determined using a rotatory basket batch adsorber. The mechanical details of this adsorber are reported elsewhere (Ocampo-Perez et al. 2017). The procedure employed is briefly described. First, 0.5 g of GAC were added to a basket, which was later anchored to the motor shaft. The stirring velocity was set to 200 rpm (higher velocities did not affect the adsorption velocity). Afterwards, a 1 L solution was rapidly added having a known initial concentration of the compounds studied. This initial concentration was varied for CA (0.57-2.27 mmol L^{-1}) and CGA (0.29-1.69 mmol L^{-1}). 1 mL aliquots were withdrawn for the system at specified time points to determine acid concentrations until reaching equilibrium. Temperature was kept at 25°C during the whole experiment by keeping the system immersed in a water bath. To study the effect of the adsorption pH on the adsorption capacity and velocity, experiments were conducted at pH values of 3, 5, and 7 (by adding 0.01 M HCl or 0.01 M NaOH). The mass of CA or CGA adsorbed was determined at each time point using Equation 1, while the equilibrium adsorption capacity was calculated using Equation 2.

$$q = \frac{V(C_{A0} - C_A(t))}{m} \quad \textbf{(1)}$$

$$q_e = \frac{V(C_{A0} - C_{Ae})}{m} \quad \textbf{(2)}$$

2.5. Mathematical models

Several mathematical models to interpret the adsorption velocity are available in the literature. These models are based on some of the three stages of mass transport that exist during the adsorption process (external mass transport, intraparticle diffusion, and adsorption on the active site. Each of these stages represent a mass transfer resistance and, as usual, the slowest stage will control the global adsorption velocity. The kinetic models consider that the global adsorption velocity is controlled by the adsorption the active site, disregarding the intraparticle diffusion and external mass transport. Moreover, the controlling stage is represented by a reaction rate. The kinetic models most employed are the first order (Lagergren equation) and second order models. Unlike the kinetic models, the diffusional models are obtained from mass balances and constitutive equations (adsorption isotherm); therefore, the mass transport parameters can be related with the operation variables.

2.5.1. First order kinetic model

The first order kinetic model is described by Equation 3 (it is solved considering that at the beginning of the adsorption process, no adsorbate exists on the particle). It considers that the adsorption is driven by a linear driving force generated from the difference between the equilibrium capacity and the existing capacity such that the process is interrupted when reaching equilibrium.

$$\frac{dq}{dt} = k_1\left(q_e - q\right) \qquad \textbf{(3)}$$

2.5.2. Second order kinetic model

The second order kinetic model is expressed in Equation 4. The same driving force of the first order model is considered but squared to indicate a faster adsorption process. The same initial condition of the first order model is used.

$$\frac{dq}{dt} = k_2\left(q_e - q\right)^2 \quad \textbf{(4)}$$

2.5.3. Intraparticle diffusion model

To evaluate the existence of diffusional phenomena during the adsorption process, the intraparticle diffusion equation is widely used in the literature. This model indicates that the adsorption capacity varies linearly with $t^{0.5}$. If the data show good linearity a pass through the origin, it can be stated that the adsorption rate is controlled by intraparticle diffusion [49,50]. Moreover, different slopes during the adsorption process establish the presence of several mass transfer resistances. The intraparticle diffusion model is presented in Equation 5.

$$q_t = k_i t^{0.5} + b \quad \textbf{(5)}$$

2.5.4. General diffusion model

The general diffusion model (PVSDM) used in this work is based on the following considerations: i) the external mass transport is described by the film theory characterized by an external mass transfer coefficient, k_L, ii) intraparticle diffusion occurs by diffusion in the pore volume (Fickian diffusion) and surface diffusion, iii) the adsorption velocity on the active site is instantaneous, and iv) the GAC particles are spherical, rigid, and isotropic. From

these considerations, mass balances of the adsorbate in the bulk solution and within the particle establish Equations 6-9.

$$V\frac{dC_A}{dt} = -mSk_L\left(C_A - C_{AP}|_{B_{p\text{-}s}}\right) \quad \textbf{(6)}$$

$$\varepsilon_p\frac{\partial C_{AP}}{\partial t} + \rho_p\frac{\partial q}{\partial t} = \nabla\cdot\left(D_{ep}\nabla C_{AP} + D_s\rho_p\nabla q\right) \quad \textbf{(7)}$$

$$t=0 \qquad C_A=C_{A0} \qquad C_{AP}=0 \quad \textbf{(8)}$$

$$-\mathbf{n}_{p-s}\cdot\left(D_{ep}\nabla C_{AP} + D_s\rho_p\nabla q\right) = k_L\left(C_A - C_{AP}|_{B_{p\text{-}s}}\right) \quad \textbf{(9)}$$

Equation 6 represents the variation of solute concentration in the solution due to the transport of solute from the solution to the external surface of the particle. The left-hand side of Equation 7 indicates that the solute inside the particle accumulates in the volume and surface of the pores. Meanwhile, the right-hand side indicates that the intraparticle diffusion of the solute can occur by diffusion in the pore volume and surface diffusion. The initial and boundary conditions (Equations 8-9) indicate that at the beginning (t = 0) there is no solute inside the pores of the particle, and there is continuity of the mass flux at the external surface of the particle (r = R).

Usually, the adsorption rate on an active site is assumed to be instantaneous; therefore, local equilibrium exists between the concentration of solute in the solution inside the pore solution ($C_{AP} = C_{Ae}$) and the mass of solute adsorbed on the pore surface. This equilibrium is represented by the adsorption isotherm, which is the mathematical relationship between q and C_{AP} (Equation 10).

$$q = f(C_{AP}) \quad \textbf{(10)}$$

2.6. Binary adsorption of CA and CGA on GAC

The experimental data of binary adsorption at equilibrium were obtained using a batch adsorber. This adsorber consists in a 50 mL centrifuge tube that contains the binary solution of known concentration and certain adsorbent mass, the tube is immersed in a constant-temperature (by a circulating fluid) water bath. The procedures to obtain data was as follows: 0.05 g of GAC were added to the tube along with the binary solution of initial concentration (varied from 0.29 to 1.69 mmol L^{-1} for CA and CGA). The initial pH value was set to 3; it was maintained by adding 0.1N HCl throughout the experiment. The system was allowed to reach equilibrium and a 1 mL sample was withdrawn to determine concentration of both acids. Finally, the adsorption capacity of GAC towards each acid was evaluated using Equation 2.

3. RESULTS AND DISCUSSION

3.1 Textural and chemical properties of GAC

The chemical properties of GAC were obtained using an acid-base titration. The concentration of total acid sites was 0.090 meq/g, while that for total basic sites was 0.486 meq/g. Therefore, the surface of GAC has a predominantly basic character. The pH value of zero charge, pH_{PZC}, resulted equal to 9.4, which indicates that pH values below 9.4 propitiate a positively charged GAC surface, while the opposite (negatively charged) occurs at pH values above 9.4. This result also corroborates the basic character of the GAC surface.

The textural properties were obtained from the experimental data of the adsorption-desorption isotherm of N_2 at 77 K (Figure 2). In this isotherm, a type I-B behavior is observed,

which is characteristic of microporous materials (a great amount of N_2 is adsorbed at low pressures). Moreover, a slight type H4 hysteresis loop can be observed, which is representative of solids with pores with narrow slit. The experimental data heled determining that the total pore volume for the material studied was 0.36 $cm^3\ g^{-1}$ (for a P/P_0 value of 0.95), which confirms that the porosity of the material is adequate. The BET equation established a specific area of 686 $m^2\ g^{-1}$, while the microporous area was 443 $m^2\ g^{-1}$ with a micropore volume of 0.32 $cm^3\ g^{-1}$ (both determined using the Dubinin-Radushkevich equation). Finally, the pore size distribution presented in Figure 2 was obtained by the DFT method, a narrow unimodal distribution is observed with a slight presence of 2-30 nm mesopores.

3.2 Individual and binary adsorption at equilibrium

The adsorption equilibrium for both acids was studied at pH values of 3, 5, and 7 (at 25 °C), at these pH values studied the adsorption capacity is expected to be affected through changes not only in the surface charge of the adsorbent but the speciation of the acids studied. Additionally, experiments at pH values above 7 were not carried out due to stability issues of both acids (Mendel Friedman and Hella S. Jurgens 2000). For the adsorption process of CA, Figure 3a shows that the adsorption isotherms have a similar behavior (type I isotherm) with a marked asymptotic tendency when increasing the equilibrium concentration irrespective of the pH value. This phenomenon might be attributed to the generation of a monolayer on the surface of the adsorbent during the adsorption process. This implies a non-existent interaction between the CA molecules adsorbed. Moreover, once an adsorption site is occupied by a molecule, it is not possible for another molecule to become adsorbed inhibiting a multilayer adsorption. This suggests that one of the adsorption mechanisms

296 involved are π-π interactions between the aromatic ring of the CA molecule and the graphitic
297 planes of GAC.

298 The adsorption capacity obtained at different pH values revealed that increasing the
299 pH value of the solution improved the adsorption process. In this regard, at an equilibrium
300 concentration of 1.2 mmol L-1 the adsorption capacity increased by 15% when the pH value
301 raised from 3 to 5. Similarly, a 50% increase was obtained when the pH values changes from
302 3 to 7. This result can be explained considering that the surface of the GAC is positively
303 charged in the pH range studied, while the CA molecule is mostly neutral at pH 3. An increase
304 in pH promotes the dissociation of CA generating negatively charged species at pH > 6. This
305 situation promotes the establishment of attractive electrostatic interactions (combined with
306 the π-π interactions) between CA and the surface of the adsorbent; therefore, increasing the
307 adsorption capacity in response to the increase in pH value of the solution.

308 For the case of CGA adsorption, a slightly different behavior is obtained when
309 compared to GA at the pH values studied. Moreover, the adsorption isotherms showed an
310 non-asymptotic behavior upon increasing the equilibrium concentration. In general, the
311 adsorption capacity of CGA at pH values of 3 and 5 resulted similar to those obtained for
312 CA, while an increase of only 15% was observed at pH 7. These results imply that despite
313 the existence of electrostatic interactions at pH 7; they do not have the same adsorption force
314 determined for the case of CA. This situation might be attributed to the nonplanar structure
315 of CGA when compared to CA (Figure 4), which ends up affecting the π-π interaction.
316 Therefore, the electrostatic forces have influence on the adsorption over the positively
317 charged adsorbent surface; nonetheless, they are not synergistic with the π-π interactions to
318 the same level found with CA, promoting less surface saturation.

The experimental adsorption data at different pH values were described by the Freundlich and Langmuir isotherm models represented by Equations 11 and 12, respectively. The optimized values of the fitting parameters were determined using nonlinear regression using Statistica®, Table 2 shows the results for each model. The R^2 values establish that the Langmuir model better represents the adsorption of CA given the asymptotic behavior of the data, while the Freundlich model better describes the data for CGA (Figure 3b).

$$q_e = \frac{q_m K C_e}{1 + K C_e} \tag{11}$$

$$q_e = k C_e^{1/n} \tag{12}$$

Figure 5 shows the experimental data for the adsorption equilibrium of the binary solution of CA and CGA on GAC at 25°C and pH set to 3. This pH value was selected considering that the residual water from the coffee production process has similar pH value (Haddis and Devi 2008; Selvamurugan et al. 2010; Alemayehu et al. 2020). The experimental data for the binary system was interpreted by the extended multicomponent Langmuir (EML) model, which is described in Equation 13.

$$q_i = \frac{q_{max} K_{E,i} C_i}{1 + \sum_{j=1}^{N} K_{E,j} C_i} \tag{13}$$

The EML model assumes that the adsorption sites on the adsorbent surface are uniform; therefore, both adsorbates compete for the same adsorption sites that are energetically equal. Table 3 shows the values of the optimized parameters from the model, q_{max} reaches a value of 1.48 mmol g^{-1}, while the values of K_{EI} demonstrate that the GAC surface has higher (almost 2-fold) affinity towards CGA when compared to CA. The

prediction of the EML model is presented in Figure 3 for both compounds where good fitting to the experimental data is observed.

The effect of CGA presence on the adsorption capacity of CA is presented in Figure 5a. In this figure, the adsorption capacity of CA is drastically reduced at CGA equilibrium concentrations less than 0.2 meq L^{-1}, whereas at higher concentrations the effect is less evident. To clarify this even further, Figure 5b presents the mass of CA adsorbed as a function of the CGA equilibrium concentration; here, the effect described is mor evident. Furthermore, at a CGA equilibrium concentration of 1 mmol L^{-1}, the adsorption capacity diminishes by 73%, which clearly indicates the preference of the GAC surface for CGA at higher equilibrium concentrations of the same.

Figures 5c and 5d show the effect of the CA presence on the CGA adsorption, it can be appreciated that the adsorption capacity diminishes in a less pronounced fashion when compared to the results obtained for the adsorption of CA. As an example, for equilibrium concentrations of 1 and 0.7 mmol L^{-1} for CA and CGA, respectively, the adsorption capacity decreases by 40% corroborating the preference of GAC for CGA. The XLogP3 values for CA and CGA are 1.2 and -0.4; therefore, the latter has a more hydrophobic character, which favors its adsorption when competing with the former. Finally, the maximum value found for q_m in the binary system lies in the range estimated for the individual system, i.e. the binary adsorption of CA and CGA is antagonistic since both acids adsorb on the same adsorption sites.

3.3 Adsorption rate of CA and CGA on GAC

Tables 4 and 5 show the operating conditions employed to obtain the adsorption kinetics for both individual acids on GAC, while Figure 6a-b shows as an example the experimental data

for CA (Exp. 1-4) and CGA (Exp. 1-5), respectively. For both acids, the adsorption capacity rapidly increases for the first 200 and 1000 min, respectively. Afterwards, the adsorption capacity slowly increases until reaching equilibrium. This behavior implies the existence of diverse mass transfer resistances during the adsorption process associated to the microporous character of the adsorbent. The equilibrium conditions were reached at approximately 1,800 and 10,000 min for CA and CGA, respectively, i.e. the adsorption rate of CA is ~5 times faster than for CGA. These results could be explained in terms of the molecular size of CGA (Table 1) that is ~2 times larger than the size of CA, which could render a slower diffusion process within the microporosity of the adsorbent for the former. Another factor to consider is the structure of the adsorbent that presents an average pore diameter of 1.21 nm; this value is close to the molecular size of CGA. Therefore, for CGA restrictive diffusional effects might exist hindering the adsorption process. Moreover, the behavior observed for CGA might also be attributed to steric effects derived from the number and position of the hydroxyl moieties in the aromatic ring (Li et al. 2010; Simanaviciute et al. 2017); this situation could induce that the adsorbed molecules restrict the diffusion of new CGA molecules, which results in a more complex adsorption mechanism with the subsequent longer equilibration times.

3.4 Interpretation of the experimental data for the adsorption rate of CA and CGA on GAC using kinetic models

The experimental data for CA and CGA were interpreted by the pseudo-first and pseudo-second order kinetic models (Equations 3 and 4), respectively. The optimized values for the parameters k_1, k_2, qe_{exp1}, and qe_{exp2} were obtained by nonlinear fitting using Scientist®, the results are shown in Tables 4 and 5 for CA and CGA, respectively. Both kinetic models

382 appropriately describe the experimental data according to the values obtained for the
383 correlation coefficient (R^2); nonetheless, the pseudo-second order model shows R^2 values
384 closer to 1 and values of q_e closer to the experimental data. Therefore, this model was selected
385 to describe the adsorption process of both compounds (See Figure 6a-b). As mentioned
386 before, the kinetic models consider that the adsorption rate is governed by the surface reaction
387 neglecting the external mass transport and intraparticle diffusion. In this sense, to evaluate
388 the existence of a correlation between k_2 and the operating conditions, Figure 7 shows the
389 variation of k_2 as a function of q_e at the different pH values studied. For the case of CA, k_2
390 did not present a tendency when increasing q_e or modifying the solution pH, which could
391 indicate the likely presence of other mass transfer resistances. On the other hand, for CGA
392 the value of k_2 diminishes exponentially upon increasing the value of q_e; this could be
393 ascribed to the availability of active sites on the adsorbent surface, which are reduced as the
394 adsorption process progresses.

395 Figure 8a-b presents as an example, the analysis of the experimental data interpreted
396 by the intraparticle diffusion model (Equation 5) for CA (Exp. 1-4) and CGA (Exp. 1-5)
397 correspondingly, while Tables 6 and 7 show the values for the intraparticle diffusion rate
398 constant (k_i), regression coefficient (R^2), and y-intercept (b) for all experiments. Considering
399 the values of the regression coefficient, the intraparticle diffusion model properly describes
400 the experimental data for both acids. Furthermore, the graphs (Figure 8) showed multi-
401 linearity, which indicates the presence of several mass transfer resistances. For CA and CGA,
402 the values of k_i were compared in three sections. Based on this, it can be inferred that at the
403 beginning (section 1) of the adsorption process the external mass transfer is important given
404 that this section shows higher values of k_i for both acids. Section 2 defines the point where

405 the adsorption velocity starts to be controlled by the intraparticle diffusion. In this case, the
406 values for ki are slightly higher for CA when compared to CGA, which could be associated
407 to the complexity of the CGA molecule (bigger size and number of hydroxyl moieties) that
408 could render a higher resistance to diffusion.

409 **3.5. Experimental data interpretation by the diffusional model**

410 The previous section established that several mass transfer resistances exist during the
411 adsorption of both acids. For this reason, the PVSDM was used to interpret the experimental
412 data. This model considers that the intraparticle diffusion occurs simultaneously in the pore
413 volume and on the surface. To solve this model, it is necessary to calculate the values for the
414 external mass transport coefficient (k_L), effective diffusion coefficient (D_{ep}), and superficial
415 diffusion coefficient (D_s).

416 The values for k_L were estimated using Equation 14, which was developed by
417 Furusawa and Smith (1973) (Furusawa and Smith 1973) for stirred tank reactors.

418

$$k_L = -\frac{V}{mS}\left[\frac{d\left(\frac{C_A}{C_{A0}}\right)}{dt}\right]_{t\to 0} \qquad \textbf{(14)}$$

419 In Equation 14, the term in square brackets is the slope of the kinetic curve at time
420 closer to zero. The values of k_L obtained for both acids are presented in Tables 8 and 9 with
421 higher values for CA when compared to CGA, which indicates higher external mass transfer
422 of CA towards the surface of GAC. These results are in line with those obtained with the
423 intraparticle diffusion model from the previous section.

The values for D_{ep} were evaluated using Equation 15 with a tortuosity factor for the GAC studied of 3.5 [54].

$$D_{ep}=\frac{D_{AB}\varepsilon_P}{\tau} \quad \textbf{(15)}$$

Substituting the values for D_{AB}, in Equation 15, reported in Table 1 and considering $\varepsilon_p = 0.554$, values of D_{ep} equal to 1.19×10^{-6} and 7.84×10^{-7} $cm^2\ s^{-1}$ were obtained for CA and CGA, respectively.

Finally, the value of D_s was obtained by fitting the PVSDM model to the experimental data using Equation 16 as objective function.

$$\text{Error} = \int_0^t \left(C_{A,exp} - C_{A,pred}\right)^2 dt \quad \textbf{(16)}$$

As an example, Figure 9 shows the experimental data for Exp. 2 for CA and Exp. 4 for CGA along with the prediction of the PVSDM model using the optimized values for D_s of 5.04×10^{-9} and 3.89×10^{-10} $cm^2\ s^{-1}$ for CA and CGA, respectively. For both cases, the model successfully describes the experimental data during the whole experiment. This methodology was replicated for all the experiments and the optimum values for D_s are compiled in Tables 8 and 9 for CA and CGA, respectively. When comparing the values for D_s for CA and CGA, the values for the former are higher than for the latter, which helps explaining the longer diffusion times for CGA.

Figures 10a and 10b show the evolution of concentration profiles within the adsorbent particle for CA (experiment 2) and CGA (experiment 4), respectively. In general, the concentration profiles are symmetrical due to the isotropy condition assumed during the

mathematical formulation and the fact the concentration gradients are higher in the external surface of the adsorbent at any moment. Additionally, the direction of the concentration gradient always points towards the center of the adsorbent particle since at this point the concentration is always smaller, if the equilibrium is not reached. Finally, as time progresses the saturation of the material increases from the outside to the inside of the particle. Similar results were obtained for the rest of the experiments for both acids (data not shown).

To further clarify the importance of both diffusion mechanisms (in the pore volume and on the surface), the surface diffusion contribution (SDC) was estimated with respect to the intraparticle diffusion using Equation 17.

$$\%SDC=\frac{\mathbf{N}_{AS}}{\mathbf{N}_{AS}+\mathbf{N}_{AP}}\times 100\ \% \quad \textbf{(17)}$$

In Equation 17, $\mathbf{N_{AS}}$ represents the mass flux due to surface diffusion and $\mathbf{N_{AP}}$ is the mass flux due to pore volume diffusion. The mass flux of each intraparticle diffusion mechanism can be calculated using the Equations 18 and 19.

$$\mathbf{N_{AP}} = -D_{ep}\nabla C_{AP} \quad \textbf{(18)}$$

$$\mathbf{N_{AS}} = -D_s\rho_p\nabla q \quad \textbf{(19)}$$

Furthermore, the magnitude of each flux can be estimated using Equations 20 and 21.

$$\mathbf{N}_{AP}=D_{ep}\sqrt{\left(\nabla C_{AP}|_r\right)^2+\left(\nabla C_{AP}|_\theta\right)^2+\left(\nabla C_{AP}|_\varphi\right)^2} \quad \textbf{(20)}$$

$$\mathbf{N}_{AS}=D_s\rho_p\sqrt{\left(\nabla q|_r\right)^2+\left(\nabla q|_\theta\right)^2+\left(\nabla q|_\varphi\right)^2} \quad \textbf{(21)}$$

Figures 11a and 11b show the surface diffusion contribution as a function of position and time for CA and CGA, respectively. The timepoints selected for analysis were 5, 10, and 20 h for CA and 17, 42, and 84 h for CGA. It is worth mentioning that the minimum values

458 for %SDC were 55.9 and 25.5% for CA and CGA, respectively; they were found at the
459 beginning of the adsorption process. These values further increased as the adsorption
460 progressed reaching values of 100% at longer timepoints. These results suggest that, for both
461 acids, both diffusion mechanisms must be considered for the scaling-up of the process.
462 Similar analyses were performed for experiments 1-12 for CA and 1-14 for CGA, the
463 optimized values for D_s are summarized in Tables 8 and 9, respectively. In general, it is
464 notable that the values of D_s for CGA are one order of magnitude smaller than those for CA,
465 which further evidenced restricted diffusional effects for CGA mainly associated to its bigger
466 molecular size. Moreover, the values of D_s did not show any tendency with respect to the pH
467 value or the mass adsorbed at equilibrium (q_e). Finally, Figure 12 shows the prediction of the
468 PVSDM model along with the experimental data where the model satisfactorily predicts the
469 dynamics of the adsorption process irrespective of the operating conditions of the system.

470 **4. CONCLUSIONS**

471 In this work, the single and binary adsorption of CA and CGA on GAC were studied. A
472 profound study of the mass transfer mechanisms during the adsorption of both acids was also
473 performed. The adsorption experiments of the individual compounds demonstrated that GAC
474 has high affinity towards them reaching maximum adsorption capacities of 1.33 and 1.62
475 mmol g^{-1} for CA and CGA, respectively. The mechanism involved during the adsorption of
476 both acids was mainly attributed to π-π and electrostatic interactions at the pH values studied.

477 The binary adsorption demonstrated that the presence of CA or CGA during the
478 adsorption of CGA or CA, respectively, detriments the adsorption capacity with a more
479 pronounce effect for CA. Moreover, the results revealed that the adsorption of both
480 compounds is antagonistic given their similarity in adsorption mechanisms.

481 The interpretation of experimental data by application of kinetic models evidenced
482 that the pseudo-second order model provided better description of the data when compared
483 to the pseudo-first order model. Moreover, the value of the kinetic constant diminishes as the
484 adsorbed amount in the equilibrium increases due to a reduction in the availability of active
485 sites. The intraparticle diffusion model corroborated the presence of several mass transfer
486 resistance during the adsorption of both acids.

487 Finally, the interpretation of the experimental data with diffusional models helped
488 establishing that the adsorption rate of both acids is governed by intraparticle diffusion, and
489 that superficial diffusion and pore volume diffusion play important roles during adsorption
490 of both compounds.

491

Declarations

Ethical approval: Not applicable.

Consent to participate: Not applicable.

Consent for publication: Not applicable.

Availability of data and materials' statement

The datasets used and/or analysed during the current study are available from the corresponding author on reasonable request

Declaration of Competing Interest

The authors declare that they have no known competing financial interests that could have influence the work reported in this paper.

Authors' contributions

Conceptualization, R.O.-P. and E.P.-O.; methodology and experimental E.E.H-P; validation, A.I.Z.-G., O.G.-O., A.G.-D., P.D.-S., and F.B.-C; formal analysis, A.I.Z-G. and R.O.-P.; investigation, R.O.-P.; writing—original draft preparation, A.I.Z.-G. and R.O.-P.; writing—review and editing, R.O.-P., A.I.Z.-G and E. P.-O. All authors read and approved the final manuscript.

Acknowledgements

This work was funded by Consejo Nacional de Ciencia y Tecnología (National Council for Science and Technology), CONACyT, Mexico, through Grant No. 1006615.

Dra. Ana I. Zárate-Guzmán thanks Consejo Nacional de Ciencia y Tecnología (National Council of Science and Technology), CONACYT, Mexico, for the support received through the "Convocatoria 2020: Estancias posdoctorales por México".

References

Alemayehu YA, Asfaw SL, Tirfie TA (2020) Management options for coffee processing wastewater. A review. J Mater Cycles Waste Manag 22:454–469. https://doi.org/10.1007/s10163-019-00953-y

Boehm HP (1994) Some aspects of the surface chemistry of carbon blacks and other carbons. Carbon N Y 32:759–769. https://doi.org/10.1016/0008-6223(94)90031-0

Carrales-Alvarado DH, Leyva-Ramos R, Martínez-Costa JI, Ocampo-Pérez R (2018) Competitive Adsorption of Dimetridazole and Metronidazole Antibiotics on Carbon Materials from Aqueous Solution. Water Air Soil Pollut 229:. https://doi.org/10.1007/s11270-018-3730-4

Chang WC, Hsieh CH, Hsiao MW, et al (2010) Caffeic Acid Induces Apoptosis in Human Cervical Cancer Cells Through the Mitochondrial Pathway. Taiwan J Obstet Gynecol 49:419–424. https://doi.org/10.1016/S1028-4559(10)60092-7

Du N, Cao S, Yu Y (2011) Research on the adsorption property of supported ionic liquids for ferulic acid, caffeic acid and salicylic acid. J Chromatogr B Anal Technol Biomed Life Sci 879:1697–1703. https://doi.org/10.1016/j.jchromb.2011.04.013

Farah A, Donangelo CM (2006) Phenolic compounds in coffee. Brazilian J Plant Physiol 18:23–36. https://doi.org/10.1590/S1677-04202006000100003

Furusawa T, Smith JM (1973) Fluid—Particle and Intraparticle Mass Transport Rates in Slurries. Ind Eng Chem Fundam 12:197–203. https://doi.org/10.1021/i160046a009

543 Haddis A, Devi R (2008) Effect of effluent generated from coffee processing plant on the
544 water bodies and human health in its vicinity. J Hazard Mater 152:259–262.
545 https://doi.org/10.1016/j.jhazmat.2007.06.094

546 J.E. Braham and R. Bressani (1970) Pulpa de Café: Composición, tecnología y utilización

547 Jiang H, Li J, Chen L, Wang Z (2020) Adsorption and desorption of chlorogenic acid by
548 macroporous adsorbent resins during extraction of Eucommia ulmoides leaves. Ind
549 Crops Prod 149:112336. https://doi.org/10.1016/j.indcrop.2020.112336

550 Kuzin, I. A. y Loskutov AI (1996) No Title. J Appl chemestry

551 Li S, Huang K, Zhong M, et al (2010) Comparative studies on the interaction of caffeic
552 acid, chlorogenic acid and ferulic acid with bovine serum albumin. Spectrochim Acta -
553 Part A Mol Biomol Spectrosc 77:680–686. https://doi.org/10.1016/j.saa.2010.04.026

554 Liudvinaviciute D, Rutkaite R, Bendoraitiene J, et al (2020) Adsorption of caffeic acid on
555 chitosan powder. Polym Bull 78:2139–2154. https://doi.org/10.1007/s00289-020-
556 03205-4

557 Mendel Friedman and Hella S. Jurgens (2000) Effect of pH on the Stability of Plant
558 Phenolic Compounds. J Agric Food Chem 2101–2110.
559 https://doi.org/10.11777/j.issn1000-3304.2017.17064

560 Moritz M, Geszke-Moritz M (2016) Amine-modified SBA-15 and MCF mesoporous
561 molecular sieves as promising sorbents for natural antioxidant. Modeling of caffeic
562 acid adsorption. Mater Sci Eng C 61:411–421.
563 https://doi.org/10.1016/j.msec.2015.12.093

564 Mota FL, Queimada AJ, Pinho SP, Macedo EA (2008) Aqueous solubility of some natural
565 phenolic compounds. Ind Eng Chem Res 47:5182–5189.
566 https://doi.org/10.1021/ie071452o

567 Ocampo-Perez R, Aguilar-Madera CG, Díaz-Blancas V (2017) 3D modeling of overall
568 adsorption rate of acetaminophen on activated carbon pellets. Chem Eng J 321:510–
569 520. https://doi.org/10.1016/j.cej.2017.03.137

570 Pettersen EF, Goddard TD, Huang CC, et al (2004) UCSF Chimera - A visualization
571 system for exploratory research and analysis. J Comput Chem 25:1605–1612.
572 https://doi.org/10.1002/jcc.20084

573 Selvamurugan M, Doraisamy P, Maheswari M (2010) An integrated treatment system for
574 coffee processing wastewater using anaerobic and aerobic process. Ecol Eng 36:1686–
575 1690. https://doi.org/10.1016/j.ecoleng.2010.07.013

576 Simanaviciute D, Klimaviciute R, Rutkaite R (2017) Equilibrium adsorption of caffeic,
577 chlorogenic and rosmarinic acids on cationic cross-linked starch with quaternary
578 ammonium groups. Int J Biol Macromol 95:788–795.
579 https://doi.org/10.1016/j.ijbiomac.2016.12.006

580 Singleton VL, Cilliers JJL (1991) Characterization of the Products of Nonenzymic
581 Autoxidative Phenolic Reactions in a Caffeic Acid Model System. J Agric Food Chem
582 39:1298–1303. https://doi.org/10.1021/jf00007a021

583 Srivastava VC, Mall ID, Mishra IM (2006) Equilibrium modelling of single and binary
584 adsorption of cadmium and nickel onto bagasse fly ash. Chem Eng J 117:79–91.
585 https://doi.org/10.1016/j.cej.2005.11.021

586 Stoeckli F, Centeno TA, Donnet JB, et al (1995) Characterization of industrial activated
587 carbons by adsorption and immersion techniques and by STM. Fuel 74:1582–1588.
588 https://doi.org/10.1016/0016-2361(95)00168-5

589 Uranga JG, Podio NS, Wunderlin DA, Santiago AN (2016) Theoretical and Experimental
590 Study of the Antioxidant Behaviors of 5-O-Caffeoylquinic, Quinic and Caffeic Acids
591 Based on Electronic and Structural Properties. ChemistrySelect 1:4113–4120.
592 https://doi.org/10.1002/slct.201600582

593 Wang Y, Ho CT (2009) Polyphenols chemistry of tea and coffee: A century of progress. J
594 Agric Food Chem 57:8109–8114. https://doi.org/10.1021/jf804025c

595

596

597

598

599

600

601

602

603

604

605

606 **Figures**

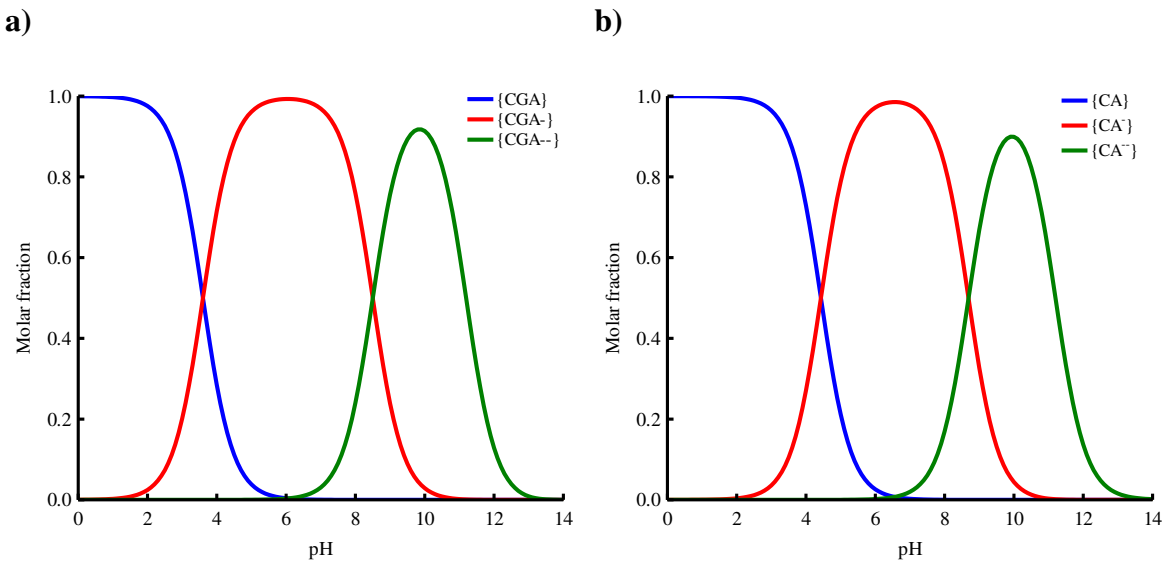

Figure 1. Speciation diagram of a) CGA and b) CA.

607

608

609

610

611

612

613

614

615

616

617

618

619

620

621

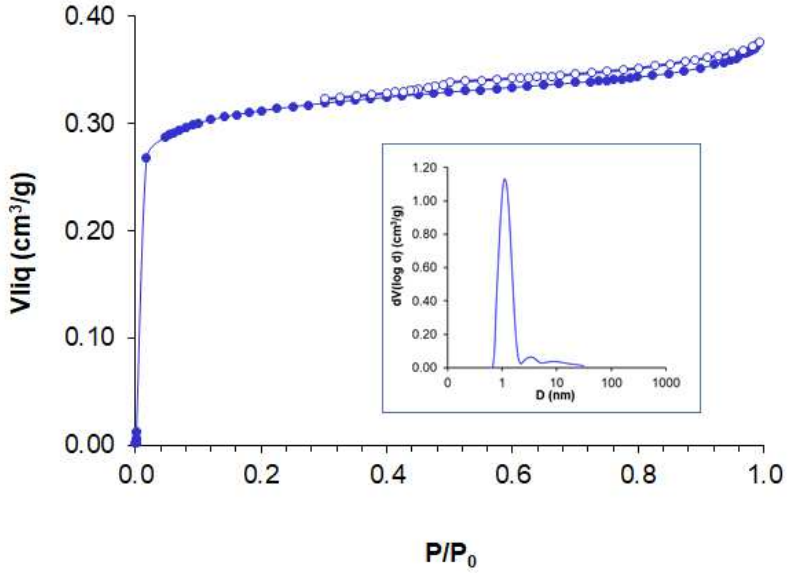

Figure 2. Adsorption-desorption isotherm of N_2 at 77 K and pore size distribution.

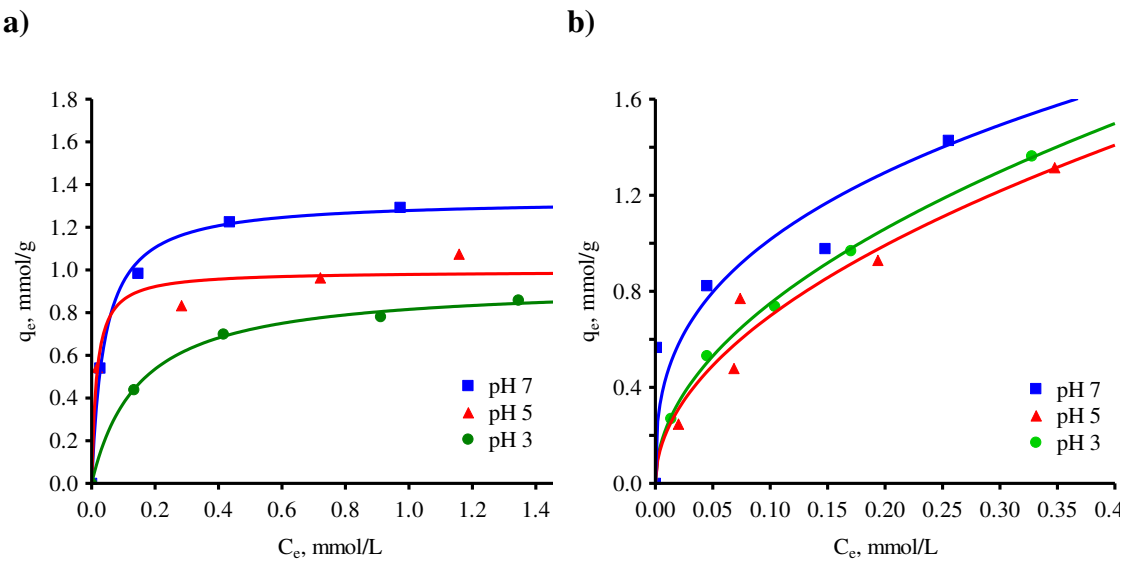

636 **Figure 3.** Adsorption isotherms for a) CA and b) CGA on GAC. The lines represent the
637 prediction of the Langmuir model for CA and Freundlich for CGA.

638
639
640
641
642
643
644
645
646
647

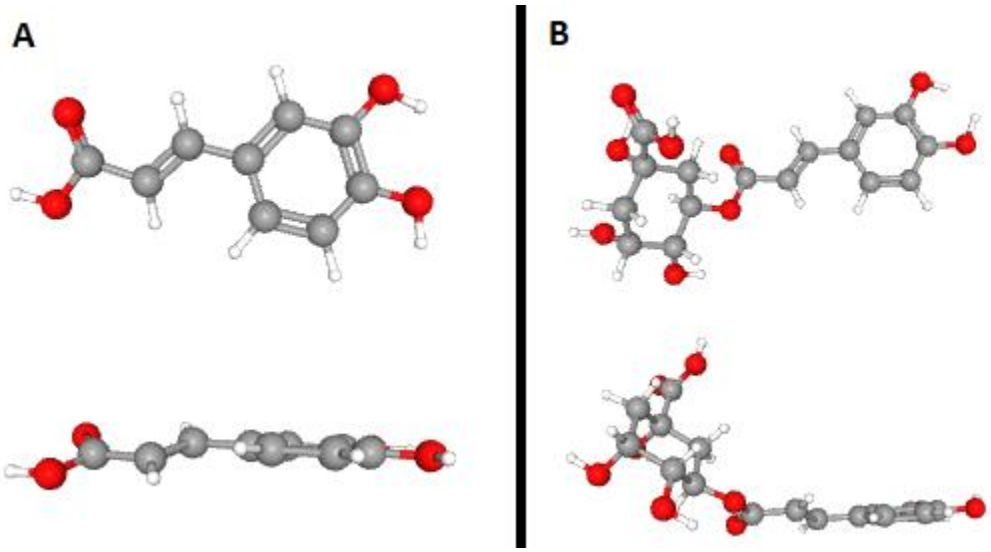

Figure 4. Chemical structure depiction of a) CA and b) CGA

668

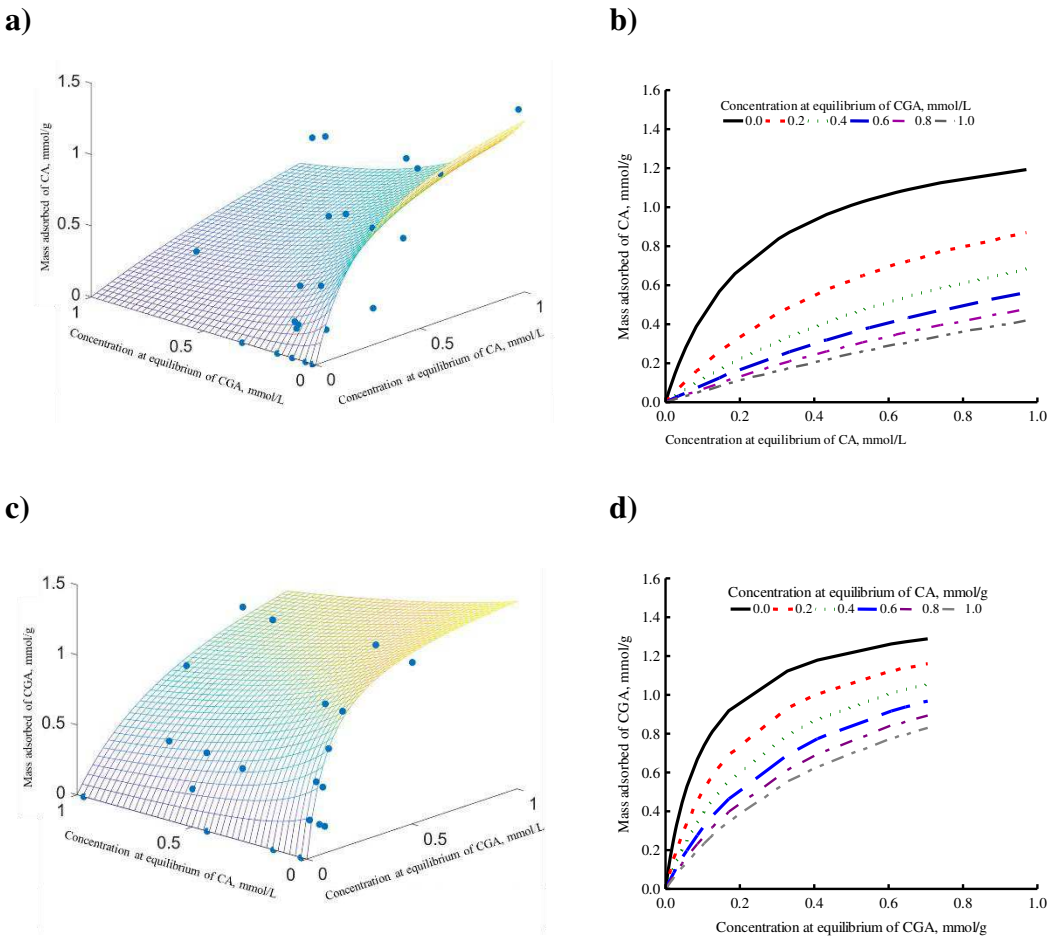

669

670 **Figure 5.** Binary adsorption isotherms of CA-CGA on GAC at 25 ° C and pH = 3.

671

672

673

674

675

676

677

678

679

a)

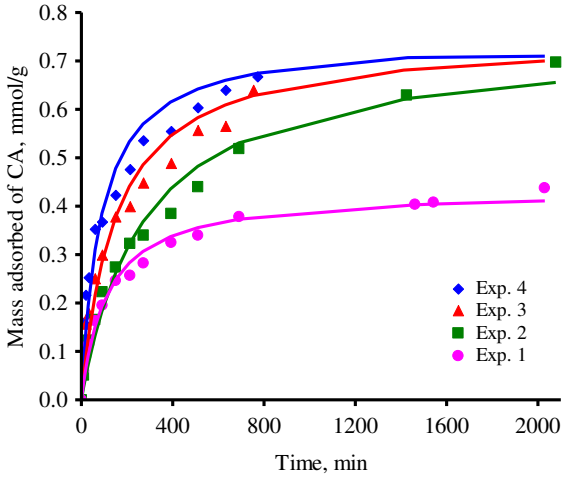

b)

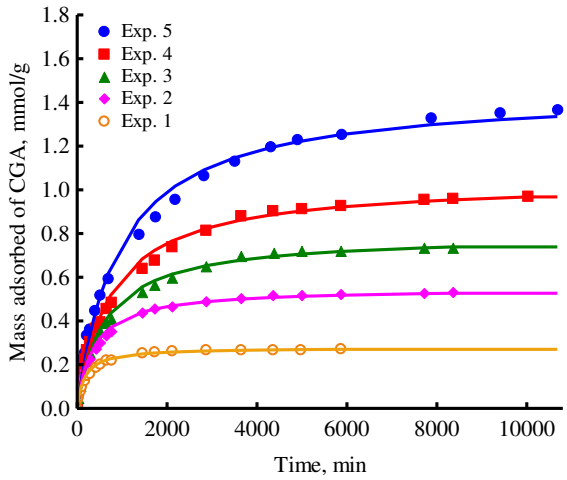

680

681 **Figure 6.** Adsorption kinetics of a) CA and b) CGA on GAC. The lines represent the

682 prediction of the second order kinetic model.

683

684

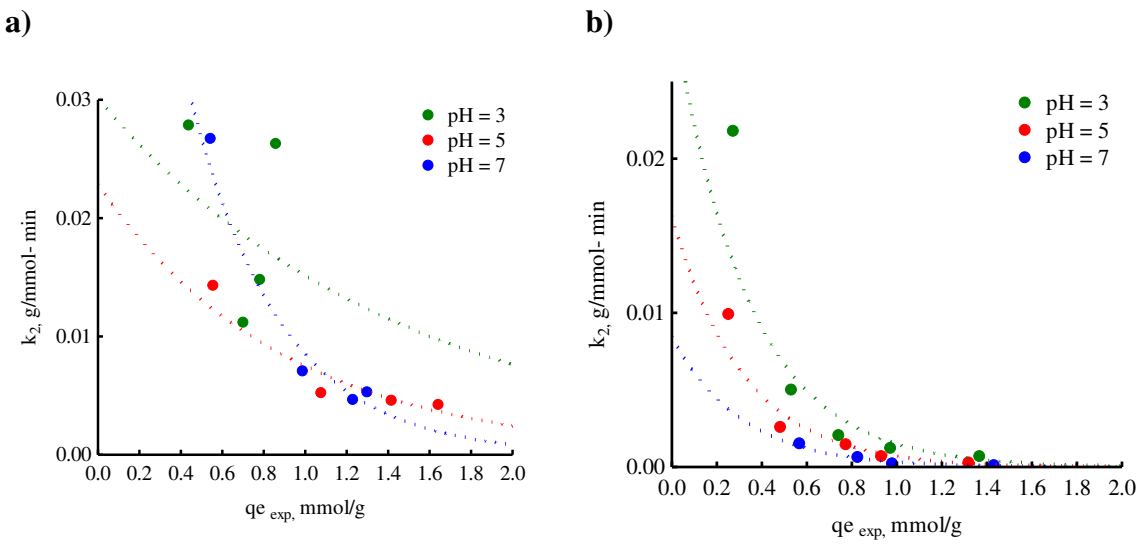

685

686 **Figure 7.** Variation of k_2 with respect to the adsorption capacity as a function of pH for a)

687 CA and b) CGA on GAC at T = 25 ° C.

688

689

690

691

692

693

694

695

696

697

698

699

700

701

702

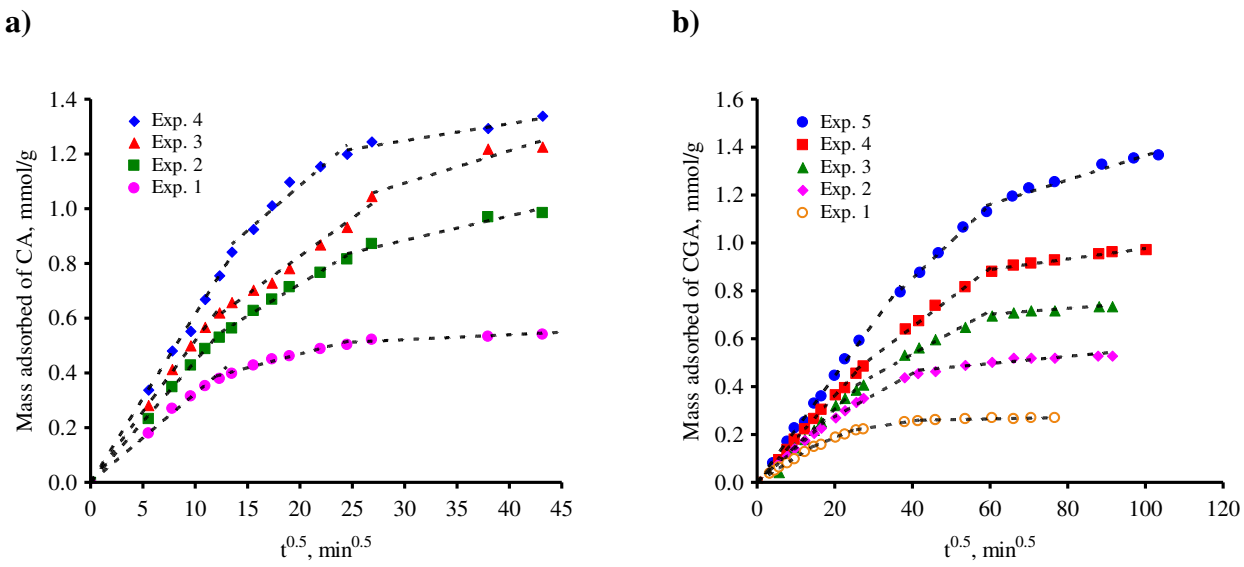

703

704 **Figure 8.** Adjustment parameters for the intraparticle diffusion model during the adsorption

705 of a) CA and b) CGA on GAC at T = 25 ° C.

706

707

708

709

710

711

712

713

714

715

716

717

718

719

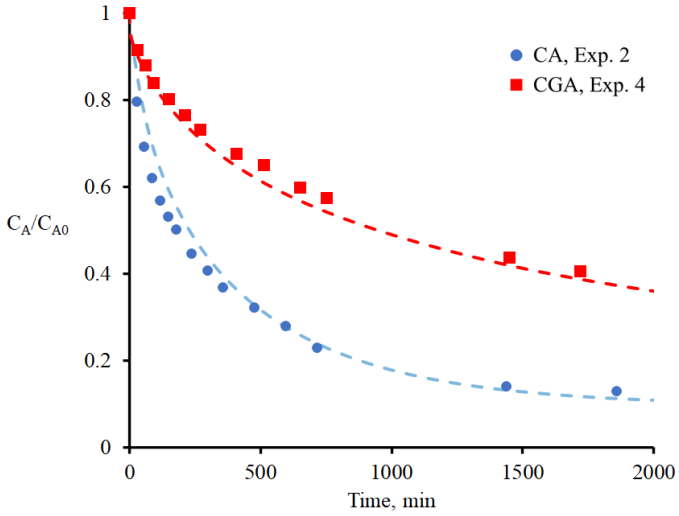

Figure 9. Decay curves of the concentration of CA and CGA, during the adsorption on GAC at T = 25 ° C. The dotted line represents the PVSDM model prediction

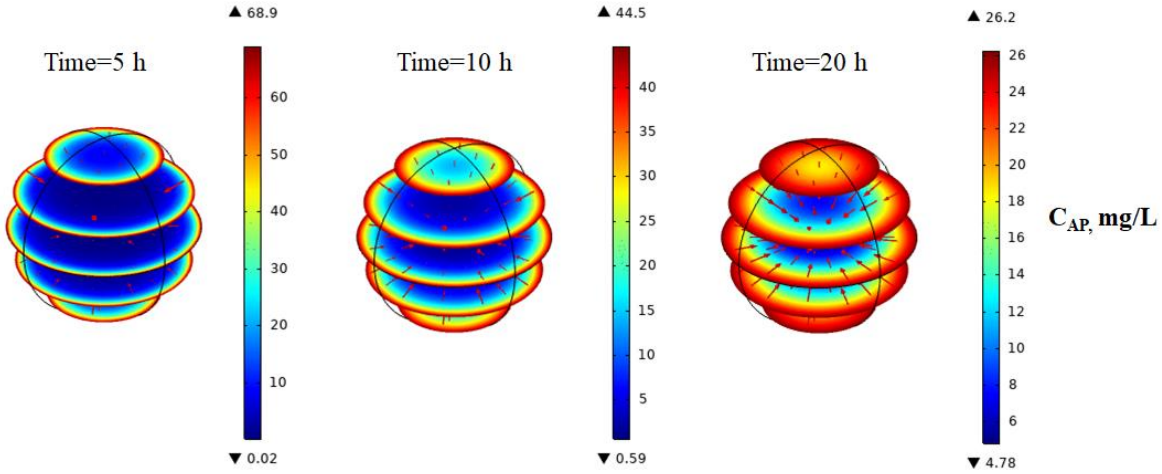

a)

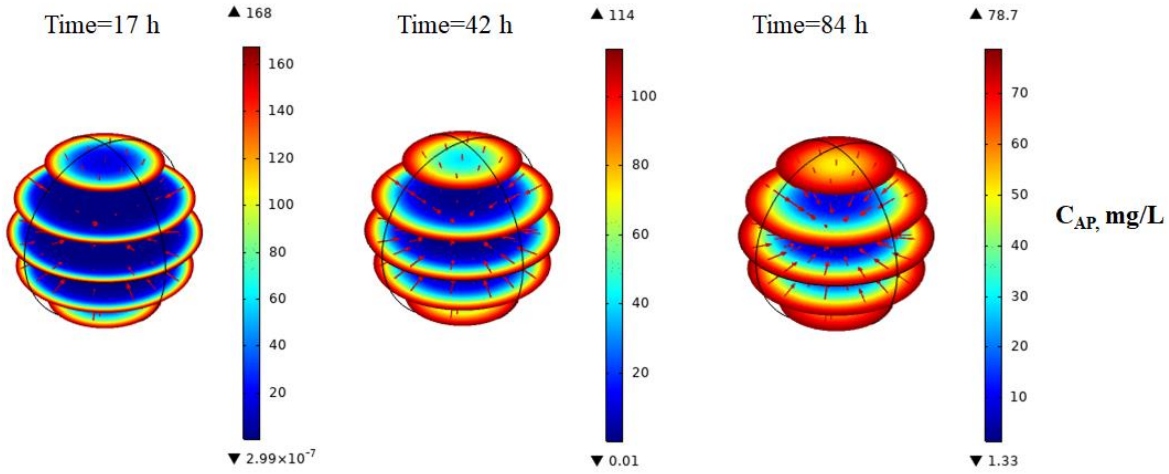

b)

735 **Figure 10.** Evolution of intraparticle concentration profiles as a function of time and position

736 for a) CA (Exp. 2) and b) CGA (Exp. 4).

737

738

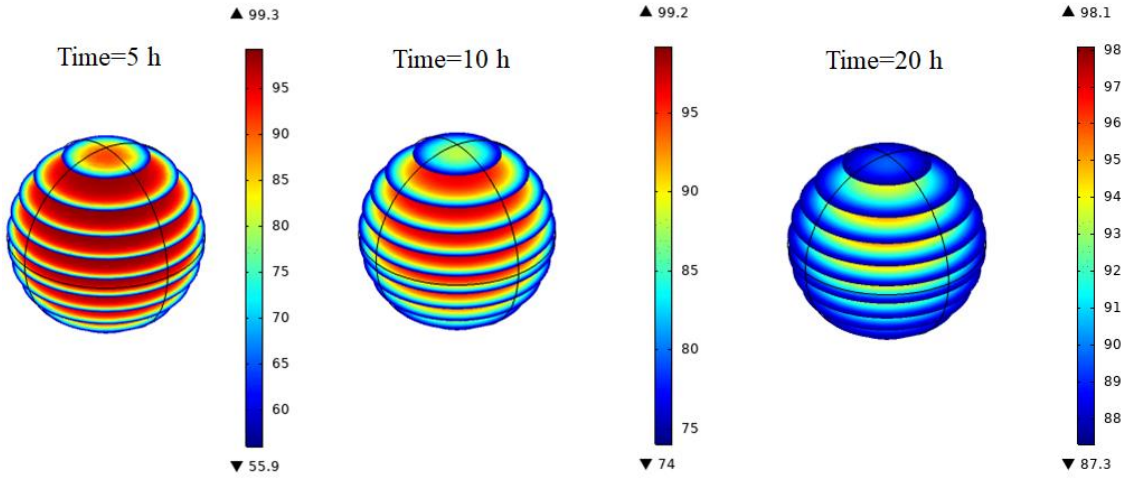

a)

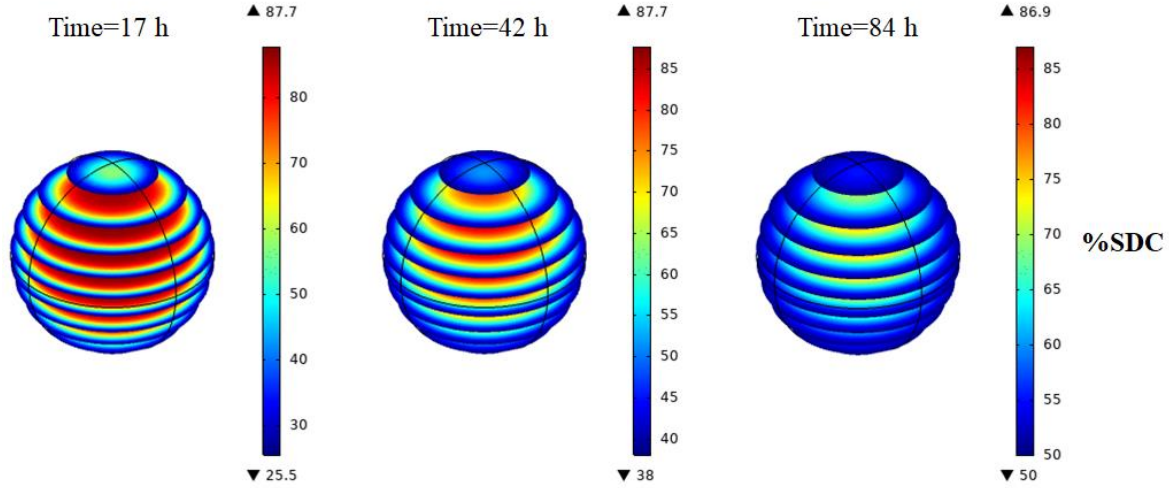

b)

739 **Figure 11.** Evolution of % SDC as a function of time and position during the adsorption of

740 a) CA (Exp. 2) and b) CGA (Exp. 4).

741

742

743

744

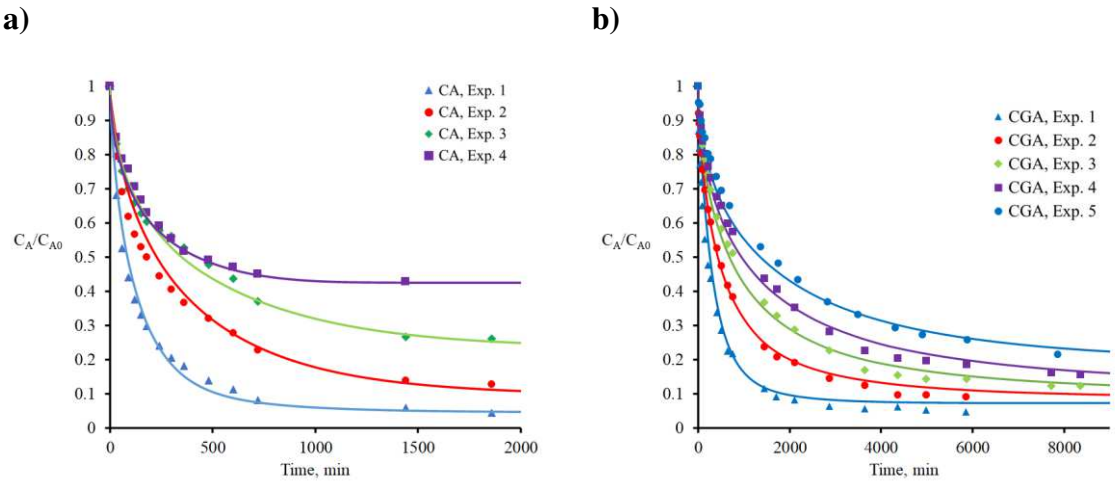

745 **Figure 12.** Decay curves of the concentration of a) CA and b) CGA during adsorption on

746 GAC at T = 25 ° C. The solid line represents the prediction of the PVSDM model.

Table 1. Physicochemical properties of phenolic acids (Pettersen et al. 2004; Mota et al. 2008; Uranga et al. 2016).

Compound	Molecular Structure	Molecular Formula	Molecular Weight (g / mol)	Solubility mg / L	pK_a	$D_{AB}\times10^6$ (cm^2/s)	Molecular Size Å	Volume $Å^3$	Área $Å^2$
CGA	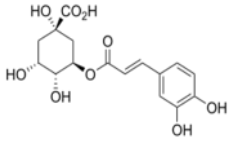	$C_{16}H_{18}O_9$	354.311	400	3.6 8.5 11.2	4.95	17.815 8.5425 6.9818	283.21	298.84
CA	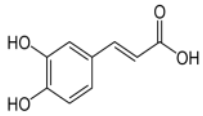	$C_9H_8O_4$	180.160	< 1000 at 22°C 980 at 25°C	4.62 8.69 11.2	7.51	12.136 6.8537 3.3191	142.53	169.35

Table 2. Adjustment parameters of the CA and CGA for adsorption isotherms on GAC at T = 25 ° C.

	pH	Langmuir			Freundlich		
		q_m mmol/g	K L/mmol	R^2	K $mmol^{1-1/n}L^{1/n}g^{-1}$	n	R^2
AC	3	0.94	6.66	0.9996	0.81	3.80	0.9976
	5	0.99	63.95	0.9933	1.04	6.15	0.9998
	7	1.33	24.38	0.9991	1.38	4.68	0.9946
ACG	3	1.84	7.51	0.9926	2.37	2.00	0.9995
	5	1.76	7.38	0.9856	2.24	1.97	0.9872
	7	1.62	25.98	0.9062	2.28	2.85	0.9867

Table 3. Adjustment parameters of the binary adsorption isotherms of CA and CGA on GAC at T = 25 ° C and pH = 3.

q_{max} (mmol/g)	$K_{E,\ ACG}$ (L/mmol)	$K_{E,\ AC}$ (L/mmol)	$q_{,\ ACG}$ R^2	$q_{,\ AC}$ R^2
1.48	9.63	4.31	0.77	0.75

Table 4. Operating conditions and adjustment parameters of the first and second order kinetic model during the adsorption of CA on GAC at T = 25 ° C.

No. Exp.	pH	C_{Ae} (mmol/L)	$q_{e,exp}$ (mmol/g)	q_e (mmol/g)	k_1 1/min	R^2	q_e (mmol/g)	k_2 (g/mmol- min)	R^2
1	3	0.57	0.44	0.3387	0.0096±0.0014	0.9900	0.4008	0.0279±0.0043	0.9966
2		1.11	0.70	0.4682	0.0062±0.0010	0.9881	0.5792	0.0112±0.0024	0.9941
3		1.69	0.78	0.5613	0.0081±0.0013	0.9858	0.6590	0.0148±0.0031	0.9936
4		2.20	0.86	0.5884	0.0131±0.0025	0.9832	0.6643	0.0263±0.0052	0.9933
5	5	0.56	0.56	0.5080	0.0058±0.0008	0.9881	0.5627	0.0143±0.0018	0.9967
6		1.12	1.08	0.7732	0.0038±0.0004	0.9897	0.8834	0.0052±0.0006	0.9968
7		1.69	1.41	0.8858	0.0037±0.0005	0.9862	1.0095	0.0046±0.0007	0.9949
8		2.24	1.64	0.9931	0.0038±0.0006	0.9841	1.1261	0.0043±0.0008	0.9927
9	7	0.57	0.54	0.5000	0.0105±0.0009	0.9961	0.5557	0.0268±0.0009	0.9998
10		1.13	0.98	0.8905	0.0058±0.0006	0.9919	1.0247	0.0071±0.0006	0.9985
11		1.66	1.23	1.0985	0.0048±0.0007	0.9838	1.2706	0.0047±0.0008	0.9939
12		2.27	1.30	1.2366	0.0065±0.0004	0.9972	1.4519	0.0053±0.0004	0.9990

Table 5. Operating conditions and adjustment parameters of the first and second order kinetic model during the adsorption of CGA on GAC at T = 25 ° C.

No. Exp.	pH	C_{Ae} (mmol/L)	$q_{e,exp}$ (mmol/g)	q_e (mmol/g)	k_1 1/min	R^2	q_e (mmol/g)	k_2 (g/mmol- min)	R^2
1	3	0.29	0.27	0.2581	0.0040±0.0004	0.9908	0.2778	0.0218±0.0020	0.9972
2		0.58	0.53	0.5007	0.0020±0.0002	0.9922	0.5497	0.0050±0.0004	0.9975
3		0.84	0.74	0.6986	0.0013±0.0001	0.9933	0.7930	0.0021±0.0001	0.9985
4		1.14	0.97	0.9154	0.0011±0.0001	0.9917	1.0402	0.0013±0.0001	0.9971
5		1.69	1.37	1.2654	0.0008±0.0001	0.9905	1.4522	0.0007±0.0001	0.9970
6	5	0.27	0.25	0.2422	0.0023±0.0002	0.9946	0.2762	0.0099±0.0009	0.9979
7		0.55	0.48	0.4558	0.0011±0.0001	0.9878	0.5217	0.0026±0.0004	0.9938
8		0.85	0.77	0.7382	0.0010±0.0001	0.9940	0.8333	0.0015±0.0001	0.9979
9		1.12	0.93	0.8991	0.0006±0.0001	0.9893	1.0426	0.0007±0.0001	0.9936
10		1.67	1.32	1.2849	0.0004±0.0001	0.9842	1.5251	0.0003±0.0001	0.9882
11	7	0.57	0.56	0.5538	0.0008±0.0001	0.9952	0.6261	0.0016±0.0002	0.9967
12		0.87	0.82	0.8004	0.0005±0.000039	0.9948	0.9353	0.0007±0.0001	0.9972
13		1.13	0.98	0.9786	0.0003±0.000016	0.9969	1.2469	0.0002±0.000022	0.9975
14		1.69	1.43	1.4956	0.0002±0.000014	0.9970	1.9992	0.0001±0.000012	0.9970

Table 6. Adjustment parameters of the intraparticle diffusion model during the adsorption of CA on GAC at T = 25 ° C.

No. Exp.	pH	Sección 1			Sección 2			Sección 3		
		k_i mmol/g-$h^{0.5}$	b_1 mmol/g	R^2	k_i mmol/g-$h^{0.5}$	b_2 mmol/g	R^2	k_i mmol/g-$h^{0.5}$	b_3 mmol/g	R^2
1	3	0.0205	-	0.9988	0.0098	0.1237	0.9857	0.003	0.2969	0.9213
2		0.0224	-	0.9935	0.0167	0.0701	0.9809	0.0093	0.2757	0.999
3		0.0318	-	0.9958	0.0162	0.1766	0.9908	-	-	-
4		0.0467	-	0.9955	0.0165	0.2284	0.9901	-	-	-
5	5	0.0243	-	0.994	0.0077	0.244	0.9685	0.0022	0.4429	0.909
6		0.0293	-	0.995	0.0117	0.3052	0.989	0.0046	0.6867	0.9507
7		0.033	-	0.9902	0.0144	0.315	0.9951	0.0078	0.7017	0.9788
8		0.0384	-	0.9836	0.0157	0.3754	0.9955	0.0101	0.7113	0.994
9	7	0.0325	-	0.9925	0.0101	0.2673	0.9673	0.0018	0.4676	0.8921
10		0.0443	-	0.9978	0.0233	0.2588	0.9884	0.0089	0.6176	0.9376
11		0.0518	-	0.9983	0.0278	0.2706	0.9844	0.0118	0.7397	0.9283
12		0.0615	-	0.9972	0.0329	0.4267	0.955	0.0062	1.0627	0.8916

Table 7. Adjustment parameters of the intraparticle diffusion model during the adsorption of CGA on GAC at T = 25 ° C.

No. Exp.	pH	Sección 1		Sección 2			Sección 3		
		k_i mmol/g-$h^{0.5}$	R^2	k_i mmol/g-$h^{0.5}$	b_2 mmol /g	R^2	k_i mmol /g-$h^{0.5}$	b_3 mmol /g	R^2
1	3	0.0105	0.9934	0.0045	0.0949	0.9279	0.0004	0.2408	0.8533
2		0.0143	0.9979	0.009	0.0948	0.9842	0.0015	0.4062	0.8706
3		0.0153	0.9875	0.009	0.1755	0.9828	0.0012	0.6307	0.9516
4		0.0181	0.9981	0.0123	0.1565	0.992	0.0022	0.7567	0.967
5	5	0.0222	0.9956	0.0155	0.2311	0.9941	0.0051	0.8549	0.9633
6		0.0066	0.9918	0.0035	0.0832	0.9849	0.0007	0.208	0.8441
7		0.0093	0.9853	0.0076	0.0232	0.9864	0.0014	0.3599	0.9036
8		0.0133	0.9982	0.0054	0.3652	0.9547	0.0015	0.6202	0.9701
9		0.013	0.9962	0.0027	0.6605	0.961	-	-	-
10		0.0177	0.8428	0.0148	0.0176	0.997	0.0048	0.7747	0.9343
11	7	0.0087	0.9964	0.0069	0.0943	0.9905	0.0008	0.4868	0.8373
12		0.0102	0.9953	0.0116	0.0385	0.9976	0.0024	0.5664	0.9689
13		0.0076	0.9596	0.0114	0.0899	0.9971	0.0035	0.5676	0.9789
14		0.009	0.922	0.0164	0.1914	0.9951	0.0062	0.7097	0.9218

Table 8. Adjustment parameters of the PVSDM model during the adsorption of CA on GAC with rp = 0.051 cm at 200 RPM and at T = 25 ° C.

No. Exp.	pH	C_{A0} (mg/L)	C_{Ae} (mg/L)	$q_{e,exp}$ (mg/g)	$k_L \times 10^3$ (cm/s)	$D_s \times 10^9$ (cm^2/s)
1	3	102.78	23.88	78.88	3.44	4.53
2		200.33	74.50	125.76	1.44	5.04
3		304.62	163.60	140.88	1.92	6.32
4		396.98	242.16	154.60	2.27	15.3
5	5	101.47	1.36	98.27	3.68	7.06
6		201.75	8.04	193.70	1.45	5.15
7		303.87	49.17	254.67	1.03	5.10
8		402.98	107.04	295.83	1.04	5.57
9	7	102.36	4.60	97.76	3.11	4.65
10		203.55	26.09	177.44	3.00	3.17
11		299.35	78.04	221.24	2.80	4.00
12		408.32	174.69	233.47	2.60	4.63

Table 9. Adjustment parameters of the PVSDM model during the adsorption of ACG on CAG with rp = 0.051 cm at 200 RPM and at T = 25 ° C.

No. Exp.	pH	C_{A0} (mg/L)	C_{Ae} (mg/L)	$q_{e,exp}$ (mg/g)	$k_L \times 10^{-4}$ (cm/s)	$D_s \times 10^{10}$ (cm^2/s)
1	3	101.30	4.74	96.56	9.40	7.81
2		203.83	15.84	187.99	9.20	5.79
3		298.15	36.78	261.37	9.00	4.74
4		404.23	60.27	343.96	8.80	3.89
5		600.20	116.12	484.08	8.60	6.11
6	5	95.47	6.89	88.58	10.5	12.6
7		193.87	24.21	169.66	1.84	2.50
8		299.75	26.08	273.67	1.91	8.80
9		398.58	68.62	329.96	1.36	7.96
10		590.15	122.98	467.17	6.77	6.32
11	7	200.36	0.29	198.17	1.81	2.04
12		308.17	15.97	292.21	1.36	6.32
13		398.74	52.19	346.55	8.87	3.00
14		597.22	90.27	506.95	7.32	4.00